

# Polynuclear Complexes Containing the Redox Noninnocent Schiff Base Ligand 2-[(*E*)-2-Mercaptophenylimino]methyl-4,6-di-*tert*-butylphenolate(2-)

Nabarun Roy,<sup>[a]</sup> Stephen Sproules,<sup>[a]</sup> Eberhard Bothe,<sup>[a]</sup> Thomas Weyhermüller,<sup>[a]</sup> and Karl Wieghardt\*<sup>[a]</sup>

**Keywords:** Schiff bases / Polynuclear complexes / Electrochemistry / Radicals / Density functional calculations

The N,O,S-donor Schiff base ligand 2-[(*E*)-(2-mercaptophenylimino)methyl]-4,6-di-*tert*-butylphenolate(2-) ( $H_2L$ ) was deprotonated with triethylamine (2 equiv.) and treated with equimolar amounts of  $Cu(OAc)_2 \cdot H_2O$ ,  $PtCl_2$ ,  $Pd(OAc)_2$ , and  $CoCl_2$ , respectively. The versatility of  $L^{2-}$  is realized in the self-assembly of four polynuclear complexes: dimeric  $[Cu^{II}_2(L)_2]$  (**1**), trimeric  $[Pt^{II}_3(L)_3]$  (**2**), and the two tetrameric complexes  $[Pd^{II}_4(L)_4]$  (**3**) and  $[Co^{III}_4(L)_6]$  (**4**), all characterized by X-ray crystallography. Electronic structure calculations (DFT) on dimeric **1** show that the two singly occupied  $Cu d_{x^2-y^2}$  orbitals are antiferromagnetically coupled, and the cal-

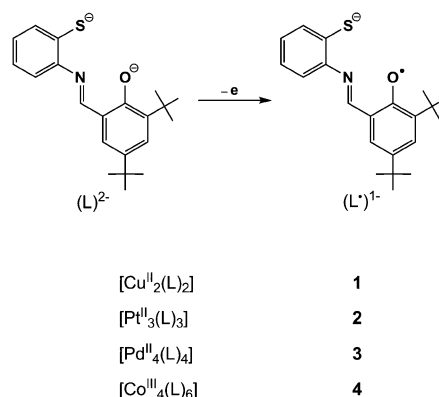
culated  $J = -724 \text{ cm}^{-1}$  agrees well with the experimental data. Complexes **3** and **4** possess several reversible one-electron, ligand-centered oxidations with electronic absorption and EPR spectroscopy displaying all the hallmarks of coordinated phenoxyl radicals. This feature further endorses our assignment of the generation of phenoxyl radicals upon oxidation and underscores the redox noninnocence of this Schiff base ligand.

(© Wiley-VCH Verlag GmbH & Co. KGaA, 69451 Weinheim, Germany, 2009)

## Introduction

Transition-metal complexes of Schiff base ligands have witnessed prodigious growth since they were first isolated in the mid 19th century principally through their use in a variety of catalytic applications.<sup>[1]</sup> However, the question of their redox noninnocence has only recently been addressed. The popular Schiff base ligand salen [*N,N'*-ethylenebis(salicylideneimino)] is a tetradentate  $N_2O_2$  donor that readily coordinates to transition metals.<sup>[2]</sup> It has long been known that the one-electron oxidation of  $Ni^{II}(\text{salen})$  is ligand centered; however, the lifetime of the product is short, either polymerizing in noncoordinating solvents<sup>[3]</sup> or tautomerizing to  $[Ni^{III}(\text{salen})]^+$  where ligating solvents stabilize a six-coordinate  $Ni^{III}$  center.<sup>[4]</sup> Furthermore, Yamauchi et al. showed that this redox tautomerism is temperature dependent, with the one-electron oxidation of  $Ni^{II}(t\text{Bu-salcn})$  [*t*Bu-salcn = *N,N'*-bis(3,5-di-*tert*-butylsalicylidene)-1,2-cyclohexanediamine] yielding  $Ni^{II}$ -phenoxyl at  $>-100^\circ\text{C}$  and  $Ni^{III}$ -phenolate  $<-120^\circ\text{C}$ .<sup>[5]</sup> The introduction of *t*Bu substituents stabilizes the phenoxyl radical and provides a steric disincentive towards polymerization. The analogous Pt complex displayed a similar temperature dependence in contrast to the Pd species, which is exclusively  $Pd^{II}$ -phenoxyl.<sup>[6]</sup>

Polynuclear complexes of Schiff base ligands are abundant in the literature owing to the ease of which they can be modified with various functional groups.<sup>[7]</sup> We have developed the tridentate N,O,S-donor ligand 2-[(*E*)-(2-mercaptophenylimino)methyl]-4,6-di-*tert*-butylphenol ( $H_2L$ ) (Scheme 1) and shown that its dianionic form coordinates to ruthenium to produce  $Ru^{III}_2(L)_2Cl_2(NCCH_3)_2$ .<sup>[8]</sup> The crystal structure of this complex showed the two  $Ru^{III}$  ions are bridged by the sulfur atom of  $L^{2-}$ , and its oxidation products are dimers with coordinated phenoxyl radicals. In this second installment, we demonstrate the versatile coordination modes of this ligand in the synthesis and characterization of a  $Cu^{II}$  dimer, a  $Pt^{II}$  trimer, and tetrameric  $Pd^{II}$



Scheme 1. Ligands and complexes.

[a] Max-Planck-Institut für Bioanorganische Chemie, Stiftstraße 34–36, 45470 Mülheim an der Ruhr, Germany  
E-mail: wieghardt@mpi-muelheim.mpg.de

Supporting information for this article is available on the WWW under <http://dx.doi.org/10.1002/ejic.200900168>.

and  $\text{Co}^{\text{III}}$  complexes. Most interestingly, these compounds exhibit reversible ligand-centered oxidations to form phenoxyl radical species.

## Results and Discussion

### Synthesis and Characterization

Several polynuclear complexes of varying geometry and nuclearity were derived from the reaction of a metal salt with the tridentate N,O,S ligand 2-[(*E*)-(2-mercaptophenylimino)methyl]-4,6-di-*tert*-butylphenol ( $\text{H}_2\text{L}$ ) in the presence of base. In a preceding paper,<sup>[8]</sup> we observed reactions with  $\text{FeBr}_2$  to give the monomeric complex  $[\text{Fe}^{\text{III}}(\text{L}-\text{L})\text{Br}]$ , where  $(\text{L}-\text{L})^{2-}$  is the disulfide bridged dimeric form of  $(\text{L})^{2-}$ , and with  $\text{RuCl}_3$  to produce dimeric  $[\text{Ru}^{\text{III}}_2(\text{L})_2\text{Cl}_2(\text{NCCH}_3)_2]$ . Here, another dimeric species is formed when  $\text{Cu}(\text{OAc})_2 \cdot \text{H}_2\text{O}$  is combined with  $\text{H}_2\text{L}$ , namely  $[\text{Cu}^{\text{II}}_2(\text{L})_2]$  (**1**). In contrast, platinum chloride reacts to give a trinuclear compound,  $[\text{Pt}^{\text{II}}_3(\text{L})_3]$  (**2**), whereas its group 10 congener, palladium, affords tetranuclear  $[\text{Pd}^{\text{II}}_4(\text{L})_4]$  (**3**). Finally, reaction with  $\text{CoCl}_2$  in the presence of air gives another tetramer,  $[\text{Co}^{\text{III}}_4(\text{L})_6]$  (**4**). All four complexes are diamagnetic and were isolated in good yields (55–77%).

### Crystal Structures of Complexes 1–4

Complexes **1–4** were characterized by X-ray crystallography and exhibit a variety of structural motifs. Table 4 gives the crystallographic data. Dimeric **1**, much like the other complexes, has its copper centers bridged by the sulfur-donor atom of  $\text{L}^{2-}$  (Figure 1). Each copper is four-coordinate, bound to one  $\text{L}^{2-}$  ligand and the sulfur atom of the adjacent ligand. The geometry of the  $\text{CuNOS}_2$  unit is almost square planar, as shown by the “trans” angles  $[\text{O}(1)-\text{Cu}(1)-\text{S}(16)$ ,  $\text{N}(9)-\text{Cu}(1)-\text{S}(46)$ ,  $\text{O}(31)-\text{Cu}(2)-\text{S}(46)$ ,  $\text{N}(39)-\text{Cu}(2)-\text{S}(16)]$  of 167.3(1), 155.6(1), 175.8(1), and 164.3(1)°, respectively, with a slight distortion towards tetrahedral.

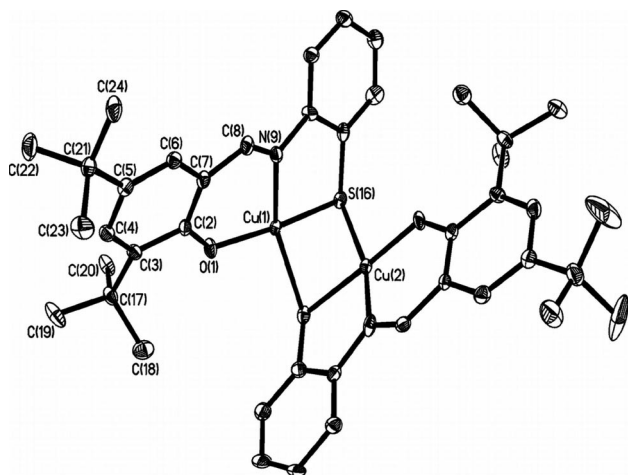
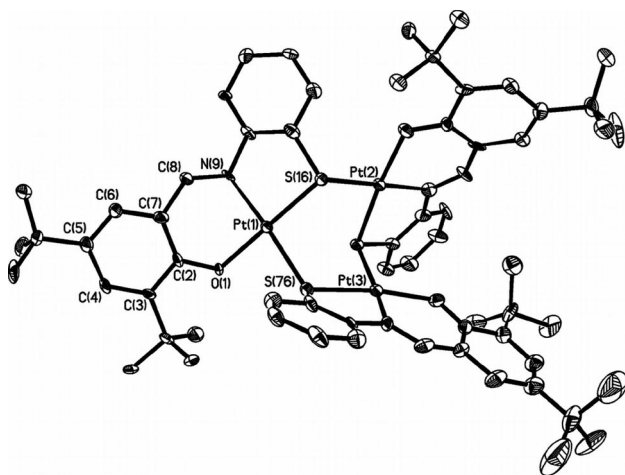
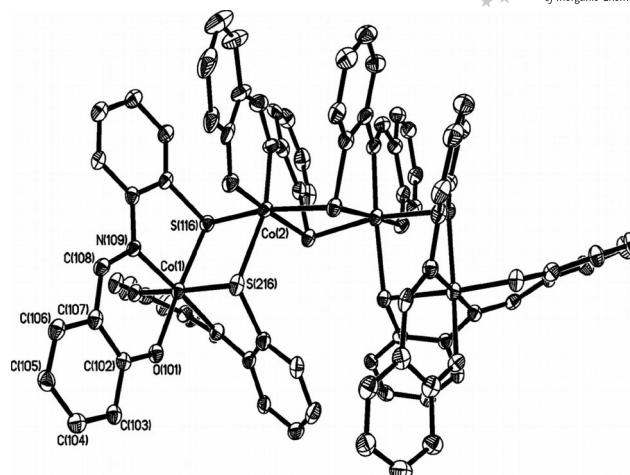
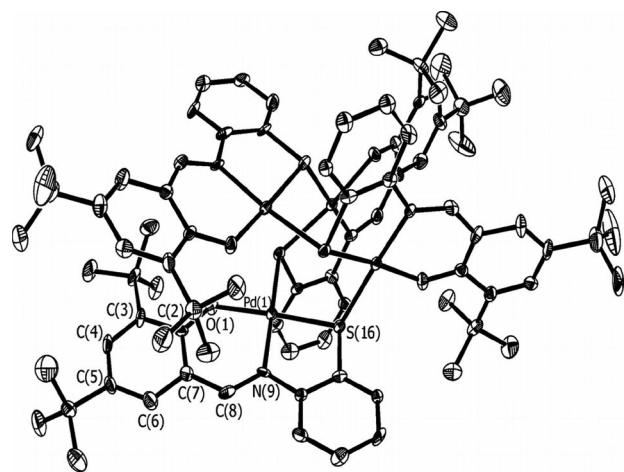


Figure 1. Perspective view of the neutral molecule in crystals of **1**.

The Cu–O and Cu–N bond lengths of 1.902(3), 1.913(3), 1.946(3), and 1.940(4) Å, respectively, are indicative of  $\text{Cu}^{\text{II}}$ , as seen with analogous salen-ligated complexes.<sup>[9]</sup> The Cu–S distances of 2.246(1), 2.329(1), 2.285(1), and 2.2318(1) Å represent the dimensions of the  $\text{Cu}_2\text{S}_2$  diamond core. This core is nonplanar, with the two  $\text{Cu}_2\text{S}_2$  mean planes resting at an angle of 80.4°. Consequently, the  $\text{Cu}(1) \cdots \text{Cu}(2)$  distance of 2.6446(8) Å is short and similar to complexes with Cu–Cu bonds. This contrasts  $[\text{Cu}_2(\text{LONO})_2]^{2-}$  [ $\text{LONO} = N$ -(2-hydroxyphenyl)salicylamide, Figure 11], where the  $\text{Cu}_2\text{O}_2$  diamond core is essentially planar and the Cu $\cdots$ Cu distance is considerably longer at 3.035(2) Å.<sup>[9]</sup> In fact, a survey of the Cambridge Structural Database revealed that this is the first complex possessing two square planar Cu centers that are near-orthogonal, with the vast majority of  $\text{Cu}_2\text{E}_2$  (E = O, S) compounds exhibiting planar diamond cores. The origin for this unique geometry is not entirely clear. There is a Cu $\cdots$ S intermolecular interaction at 3.2 Å between adjacent dimers. This, in conjunction with the steric bulk of  $\text{L}^{2-}$ , is the probable cause of the observed geometry.

Complex **2** is trinuclear, and like **1**, each platinum center is four-coordinate with its coordination sphere completed by one  $\text{L}^{2-}$  ligand and a fourth ligand, a sulfur atom from the neighboring  $\text{L}^{2-}$  (Figure 2). Despite their rarity, platinum complexes with bridging sulfur ligands are known.<sup>[10–12]</sup> Each Pt is nearly square planar, with trans angles ranging from 167.5(2) to 178.9(3)° indicating a slight distortion towards square pyramidal. The Pt ion lies, on average, 0.029 Å out of the  $\text{NOS}_2$  equatorial plane. These square planes are orientated with dihedral angles of 52.5, 63.5, and 88.0° with respect to each other, which results in a hexagonal void enclosed within the  $\text{Pt}_3\text{S}_3$  ring in a pseudochair conformation. Similar conformations were observed in the  $\{\text{PtS}\}_3$  units of  $[\text{Pt}^{\text{II}}\text{Ph}_2(\text{S}(\text{CH}_3)_2)_3]$ ,<sup>[10]</sup>  $[\text{Pt}^{\text{II}}(\text{SC}_6\text{H}_4\text{SC}_6\text{H}_4)_3]$ ,<sup>[11]</sup> and trinuclear platinum cubanes.<sup>[12]</sup> The N,O-donor atoms reside on the periphery. The  $\text{Pt}(1) \cdots \text{Pt}(2)$  and  $\text{Pt}(1) \cdots \text{Pt}(3)$  distances are similar (3.92 and 3.95 Å, respectively), whereas the  $\text{Pt}(2) \cdots \text{Pt}(3)$  distance is considerably shorter at 3.37 Å, though outside the range of a metal–metal bond. The Pt–S, Pt–O, and Pt–N average bond lengths of 2.28, 2.03, and 2.01 Å, respectively, are typical for  $\text{Pt}^{\text{II}}$  complexes with similar coordination spheres.<sup>[6,13]</sup>

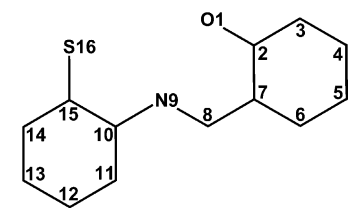
Tetrameric  $[\text{Pd}^{\text{II}}_4(\text{L})_4]$ , like **2**, consists of Pd ions in four-coordinate square planes divided into two near-parallel sets (Figure 3), with the angle between Pd(1) and Pd(3) square planes at 10.7° and a similar value of 9.9° for the square planes with Pd(2) and Pd(4) at their center. Hence, these two sets are orthogonal to each other. The palladium sits on average 0.104 Å out of the  $\text{NOS}_2$  equatorial plane, indicating a slight distortion towards square pyramidal. This displacement is directed to the opposing Pd ion giving a  $\text{Pd}(1) \cdots \text{Pd}(3)$  distance of 3.40 Å and a  $\text{Pd}(2) \cdots \text{Pd}(4)$  distance of 3.37 Å. The remaining intermetal distances are ca. 3.9 Å, with the Pd ions sitting at the vertices of a tetrahedron where the four longer edges possess a bridging sulfur atom. The average Pd–N, Pd–O, and Pd–S bond lengths of 2.00, 2.02, and 2.28 Å have likewise been observed in other  $\text{Pd}^{\text{II}}$  complexes with such ligands.<sup>[6,13]</sup>

Figure 2. Structure of the neutral molecule in crystals of **2**.Figure 4. Structure of the neutral molecule in crystals of **4**.Figure 3. Perspective view of the neutral molecule in crystals of **3**.

The other tetrameric complex,  $[\text{Co}^{\text{III}}_4(\text{L})_6]$ , consists of a four-membered chain of edge-sharing octahedra, each connected by two bridging sulfur atoms from two  $\text{L}^{2-}$  ligands (Figure 4). For the two terminal octahedra, the coordination sphere is completed by N- and O-donors from two  $\text{L}^{2-}$  ligands bound meridionally, whereas the bridging octahedra are coordinated by only one meridional  $\text{L}^{2-}$ . Thus, given the six  $\text{L}^{2-}$  ligands, the cobalt ions are in the +III oxidation state to equate with the overall neutral charge. The average Co–N, Co–O, and Co–S bond lengths (1.93, 1.93, and 2.28 Å, respectively) are consistent with such a cobalt oxidation state assignment.<sup>[14]</sup>

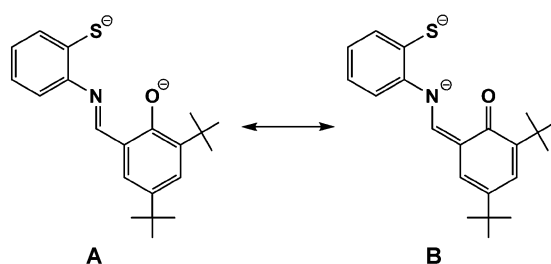
Each of the three  $\text{Co}_2\text{S}_2$  diamond cores is planar and the two terminal units make a dihedral angle of 68.9 and 89.8°, respectively, to the central  $\text{Co}_2\text{S}_2$  moiety. It has been shown for  $[\text{Ru}^{\text{III}}(\text{L})_2\text{Cl}_2(\text{NCCH}_3)_2]$  that the dimensions of its  $\text{Ru}_2\text{S}_2$  core were such that the two  $\text{Ru}^{\text{III}}$  ions form a metal–metal bond.<sup>[8]</sup> Here, the  $\text{Co}\cdots\text{Co}$  distance of ca. 3.4 Å is substantially longer than the  $\text{S}\cdots\text{S}$  distance at ca. 3.0 Å, a consequence of the low-spin  $d^6$  electron configuration of the  $\text{Co}^{\text{III}}$  ion that need not engage in such bonds.

The averaged intraligand bond lengths for complexes **1–4**, along with those in the crystallographically characterized ligand dimer,  $\text{H}_2(\text{L–L})$ ,<sup>[8]</sup> are listed in Table 1. Despite solvent disorder in complexes **2** and **3** leading to lower quality structures, the bond lengths in the phenolate arm of  $\text{L}^{2-}$  exhibit the hallmark distortion of a phenoxyl radical; two short and four long C–C aromatic bond lengths as well as a short C–O bond. Such a pattern is absent in the free ligand. In contrast, the aminothiophenolate moiety displays near-equidistant C–C bonds. We have observed this phenomenon with  $[\text{Fe}^{\text{III}}(\text{L–L})\text{Br}]$  and  $[\text{Ru}^{\text{III}}_2\text{Cl}_2(\text{NCCH}_3)_2]$ ,<sup>[8]</sup> where the intraligand bond length pattern also suggested

Table 1. Intraligand bond lengths [Å] for  $\text{H}_2(\text{L–L})$ <sup>[8]</sup> and averaged distances for **1–4**.


	$\text{H}_2(\text{L–L})$	<b>1</b>	<b>2</b>	<b>3</b>	<b>4</b>
O(1)–C(2)	1.348(1)	1.303	1.299	1.311	1.307
C(2)–C(7)	1.407(1)	1.428	1.415	1.425	1.419
C(2)–C(3)	1.408(1)	1.446	1.443	1.451	1.445
C(3)–C(4)	1.391(1)	1.380	1.383	1.378	1.380
C(4)–C(5)	1.406(1)	1.416	1.407	1.413	1.412
C(5)–C(6)	1.378(1)	1.361	1.384	1.360	1.364
C(6)–C(7)	1.403(1)	1.418	1.415	1.428	1.420
C(7)–C(8)	1.444(1)	1.425	1.438	1.428	1.423
C(8)–N(9)	1.286(1)	1.305	1.290	1.311	1.301
N(9)–C(10)	1.408(1)	1.432	1.448	1.439	1.432
C(10)–C(15)	1.391(1)	1.386	1.388	1.388	1.392
C(10)–C(11)	1.401(1)	1.403	1.384	1.399	1.397
C(11)–C(12)	1.387(1)	1.372	1.398	1.384	1.386
C(12)–C(13)	1.392(1)	1.393	1.387	1.397	1.389
C(13)–C(14)	1.389(1)	1.374	1.366	1.389	1.384
C(14)–C(15)	1.387(1)	1.399	1.408	1.388	1.390
C(15)–S(16)	1.774(1)	1.764	1.781	1.787	1.772

the presence of a phenoxyl radical coordinated to the metal. However, an examination of two ligand resonance structures (**A** and **B**, Scheme 2) displays a mechanism by which the distortion manifests without the existence of a radical. The C–O bond length in complexes **1–4** lies in the range 1.299–1.311 Å, considerably shorter (at the 3σ level) than the same bond [1.348(1) Å] in H<sub>2</sub>(L–L). Thus, upon coordination of L<sup>2–</sup> to the metal in **1–4**, the abundance of canonical form **B** is increased, which causes the experimental intraligand bonding pattern.



Scheme 2. Resonance structures **A** and **B** of L<sup>2–</sup>.

### Electrochemistry and EPR Spectroscopy

The redox properties of complexes **1–4** were investigated by cyclic voltammetry recorded at 22 °C in dichloromethane solutions containing 0.10 M [N(*n*Bu)<sub>4</sub>]PF<sub>6</sub> as supporting electrolyte at a glassy carbon working electrode. All redox potentials are referenced vs. the ferrocenium/ferrocene (Fc<sup>+</sup>/Fc) couple. The cyclic voltammograms (CVs) of **3** and **4** display rich redox chemistry, whereas oxidation of **1** and **2** led to unstable species even at low temperatures. The CVs of **3** and **4** are depicted in Figure 5 overlaid with their square-wave voltammograms to distinguish the individual oxidation processes. The potentials are similar to analogous studies of coordination complexes with pendant phenolate ligands, where oxidation clearly generates a phenoxyl radical,<sup>[15,16]</sup> and the number of oxidations is equivalent to the number of L<sup>2–</sup> ligands in each tetramer. For **3**, four reversible, ligand-centered oxidations at 0.53, 0.68, 0.85, and 0.92 V are observed. In the CV, the latter two oxidation potentials are very close to each other and manifest as a shoulder; however, they are clearly resolved in the square-wave voltammogram. For **4**, the six ligand-centered oxidations occur at 0.15, 0.44, 0.53, 0.74, 0.93, and 0.96 V, where the 30 mV difference in the latter for the two oxidations are almost indistinguishable even in the square-wave plot.

UV/Vis spectroelectrochemistry was conducted on complexes **3** and **4**, where only the first three oxidation processes of each complex were available by controlled potential coulometry, as the oxidations of the latter ligand occur within a very small potential range. The spectra depicted in Figure 6 exhibit the hallmarks of coordinated phenoxyl radicals and the electronic absorption data are listed in Table 2. Complex **3** has one prominent phenolate π→π\*

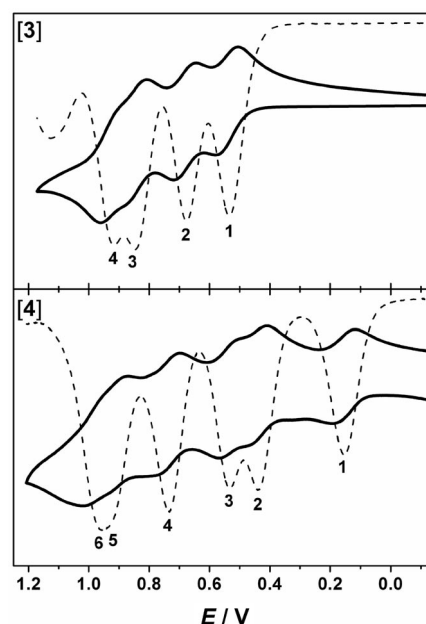


Figure 5. Cyclic (solid line) and square-wave (dashed line) voltammograms of complexes **3** and **4** in CH<sub>2</sub>Cl<sub>2</sub> solution containing 0.10 M [N(*n*Bu)<sub>4</sub>]PF<sub>6</sub> as the supporting electrolyte at 22 °C at a glassy carbon working electrode and a scan rate of 100 mV s<sup>–1</sup>. Potentials are referenced vs. Fc<sup>+</sup>/Fc.

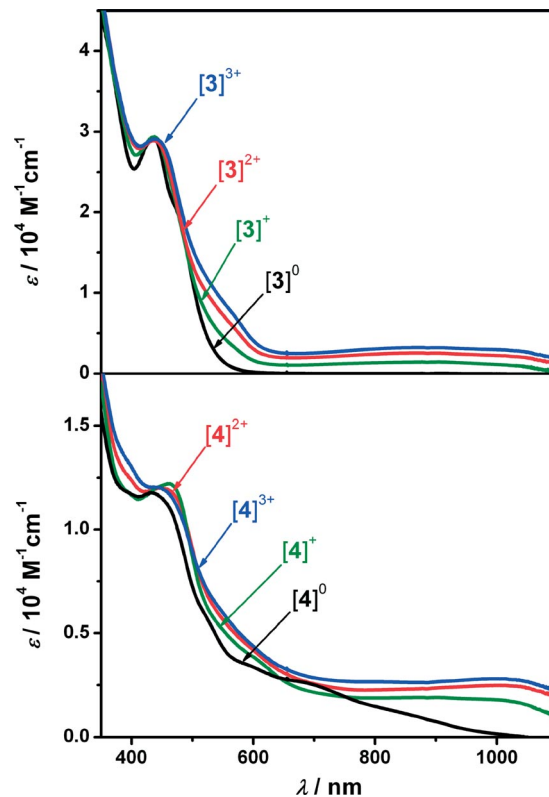


Figure 6. Electronic absorption spectra of **3** (top) and **4** (bottom) and their coulometrically generated oxidized forms in CH<sub>2</sub>Cl<sub>2</sub> solutions containing 0.10 M [N(*n*Bu)<sub>4</sub>]PF<sub>6</sub> as the supporting electrolyte at –20 °C.



Table 2. Electronic absorption data recorded in CH<sub>2</sub>Cl<sub>2</sub>.

	$\lambda$ / nm ( $\epsilon$ / 10 <sup>4</sup> M <sup>-1</sup> cm <sup>-1</sup> )	<i>S</i>
[1]	435 (1.80), 555 (sh., 0.42), 804 (0.12)	0
[2]	367 (sh., 2.39), 475 (1.32), 740 (0.02)	0
[3]	435 (2.92), 469 (sh., 2.11)	0
[3] <sup>+</sup>	439 (2.90), 542 (sh., 0.53), 878 (0.14)	1/2
[3] <sup>2+</sup>	437 (2.89), 554 (sh., 0.69), 880 (0.25)	0
[3] <sup>3+</sup>	437 (2.94), 565 (sh., 0.77), 879 (0.32)	1/2
[4]	433 (1.18), 509 (sh., 0.65), 573 (sh., 0.37), 665 (sh., 0.27), 800 (sh., 0.15)	0
[4] <sup>+</sup>	391 (sh., 1.18), 461 (1.22), 525 (sh., 0.62), 582 (sh., 0.42), 873 (0.19)	1/2
[4] <sup>2+</sup>	387 (sh., 1.29), 447 (1.20), 533 (sh., 0.64), 1002 (0.25)	0
[4] <sup>3+</sup>	391 (sh., 1.34), 446 (1.20), 540 (sh., 0.64), 994 (0.28)	1/2

transition at 435 nm ( $\epsilon = 2.9 \times 10^4 \text{ M}^{-1} \text{ cm}^{-1}$ ) with an absorption minimum at 403 nm. Upon successive, one-electron oxidation of the bulk solution, the intensity of the phenolate  $\pi \rightarrow \pi^*$  transition diminishes slightly, whereas the absorption at 400 nm becomes less pronounced as the phenoxyl  $\pi \rightarrow \pi^*$  transition develops.

Furthermore, each of the oxidized species possesses a very broad band in the near-IR region ( $\approx 950 \text{ nm}$ ), resembling previously observed trends.<sup>[15]</sup> The cobalt tetramer, **4**, displays similar trends as **3**, with a reduction in the ca. 440 nm phenolate  $\pi \rightarrow \pi^*$  transition intensity combined with the establishment of a phenoxyl  $\pi \rightarrow \pi^*$  transition that manifests as a shoulder at 390 nm.

The one-electron oxidation products, [3]<sup>+</sup> and [4]<sup>+</sup>, as well as the third oxidation product of the cobalt tetramer, [4]<sup>3+</sup>, are all EPR-active with  $S = 1/2$  ground states. EPR spectra were recorded on the coulometrically generated samples in dichloromethane at 80 K, and the spectroscopic data is displayed in Table 3. The EPR spectrum of [3]<sup>+</sup> is rhombic and centered at  $g \approx 2.007$ , characteristic of ligand-centered radical (Figure 7), similar to [Pd<sup>II</sup>(*t*Bu-salcn')].<sup>[6]</sup> The  $g$  anisotropy,  $\Delta g = 0.030$ , is significantly larger than the anisotropy observed for free phenoxyls ( $\Delta g = 0.008$ ),<sup>[17]</sup> such that despite the lack of any observable metal hyperfine (<sup>105</sup>Pd,  $I = 5/2$ , 22.3% natural abundance), which is not uncommon amongst paramagnetic palladium(II) complexes with radical ligands,<sup>[6,18]</sup> [3]<sup>+</sup> is formulated as [Pd<sup>II</sup><sub>4</sub>(L')(L)<sub>3</sub>]<sup>+</sup>, where the phenoxyl is coordinated to the metal. The experimental anisotropy results from the large spin-orbit coupling of the metal ( $\xi_{\text{Pd}} = 1460 \text{ cm}^{-1}$ ).<sup>[19]</sup>

Table 3. EPR spectroscopic data recorded in frozen CH<sub>2</sub>Cl<sub>2</sub> solutions.

	$g_1$	$g_2$	$g_3$	$\langle g \rangle$ <sup>[a]</sup>
[3] <sup>+</sup>	2.021	2.010	1.991	2.007
[4] <sup>+</sup>	2.005	2.005	2.005	2.005
[4] <sup>3+</sup>	2.010	1.995	1.995	2.000

[a]  $\langle g \rangle = (g_1 + g_2 + g_3)/3$ .

The EPR spectra of [4]<sup>+</sup> and [4]<sup>3+</sup> are quite different to that of [3]<sup>+</sup>, most noticeably in their enormous linewidths of 21.5 and 26.9 mT, respectively (Figure 8). The average  $g$

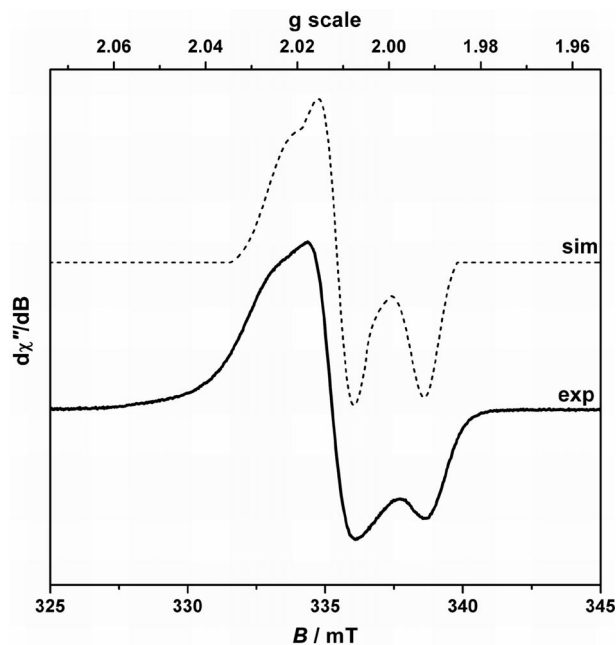


Figure 7. X-band EPR spectra of coulometrically generated [3]<sup>+</sup> in CH<sub>2</sub>Cl<sub>2</sub> at 80 K (experimental conditions: frequency 9.28 GHz; modulation 1.0 mT; power 0.10 mW).

value is consistent with a phenoxyl radical, whereas the small anisotropy is a combination of the large linewidth and spin-orbit coupling of cobalt(III) ( $\xi_{\text{Co}} = 580 \text{ cm}^{-1}$ ).<sup>[19]</sup> Again, no hyperfine is observed, though given the 100% natural abundance of <sup>59</sup>Co ( $I = 7/2$ ), it is expected. We surmise that metal hyperfine is causing the large linewidth, resulting from the overlap of eight lines per  $g$  value, as well as coupling to adjacent Co<sup>III</sup> centers. Thus, the resolution at X-band is insufficient to distinguish the metal hyperfine contribution and we define the one-electron oxidized species as [Co<sup>III</sup><sub>4</sub>(L')(L)<sub>5</sub>]<sup>+</sup>, where the phenoxyl radical is bound to the metal. Likewise, [4]<sup>3+</sup> is formulated as [Co<sup>III</sup><sub>4</sub>(L')(L)<sub>3</sub>]<sup>3+</sup>, with an axial distribution of the  $g$  tensor as a result of the interaction of all four Co<sup>III</sup> ions with three ligand radicals. The  $S = 1/2$  ground state results from coupling of two ligand radicals and infers the radicals are delocalized throughout the tetramer.

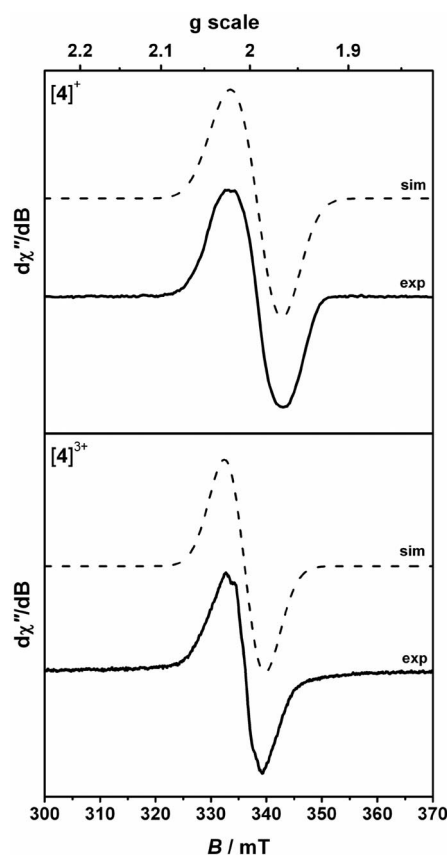


Figure 8. X-band EPR spectra of coulometrically generated (a)  $[4]^+$  and (b)  $[4]^{3+}$  in  $\text{CH}_2\text{Cl}_2$  at 10 K (experimental conditions, (a): frequency 9.43 GHz; modulation 1.0 mT; power 0.05 mW; (b): frequency 9.43 GHz; modulation 1.0 mT; power 0.025 mW).

### DFT Calculations of **1**

Density functional theoretical (DFT) calculations were performed on **1** with the *t*Bu group truncated to decrease computation time. Geometry optimization by using the B3LYP functional and a BS(1,1)  $M_s = 1$  state yielded a structure with Cu–O, Cu–N, and Cu–S bonds lengths within 0.02–0.07 Å of the experiment, typical of this functional. The intraligand bond lengths are in excellent agreement with the experiment, exhibiting short C–O bond lengths and two short and four long C–C pattern in the phenolate rings. The Cu...Cu distance increased to 3.003 Å and the dihedral angle between the Cu square planes is significantly more obtuse at 120.6°. Furthermore, the angle between the two  $\text{Cu}_2\text{S}$  planes has increased as the  $\text{Cu}_2\text{S}_2$  core has become less puckered.

The MO manifold shown in Figure 9 shows two metal-based singly occupied orbitals (SOMOs) that possess 52% Cu d character. The Mulliken spin density population analysis shows one  $\alpha$ -spin electron on the Cu(1) square plane antiferromagnetically coupled with a  $\beta$ -spin on the Cu(2) square plane, with an orbital integral overlap of  $S = 0.18$ .

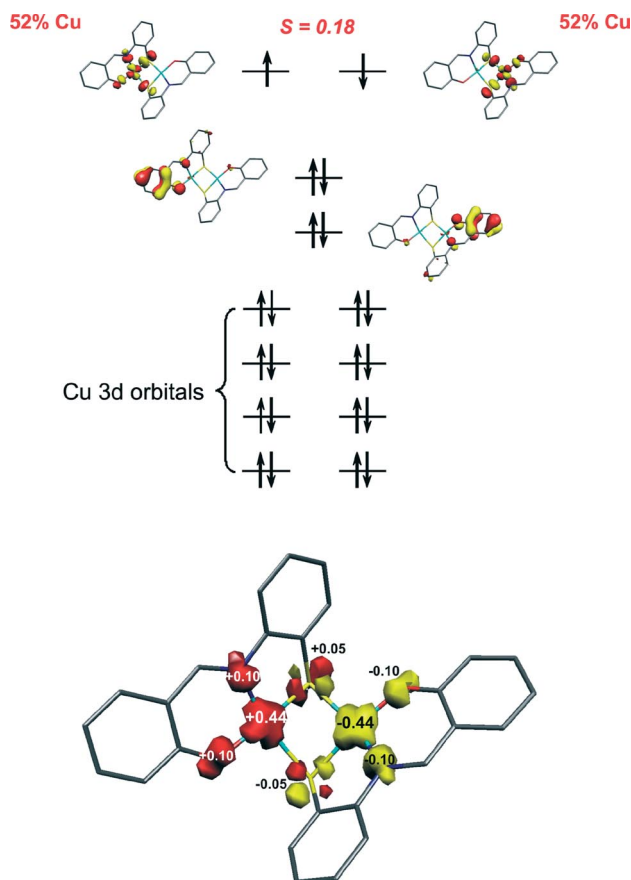


Figure 9. Qualitative MO scheme (top) for neutral **1** ( $S = 0$ ) as derived from a spin-unrestricted BS(1,1) DFT calculation. Spin density plot (bottom) from Mulliken population analysis. (Red:  $\alpha$ -spin; yellow:  $\beta$ -spin).

The exchange coupling constant, determined from the high-spin and broken symmetry (BS) energies together with the corresponding spin-expectation values  $\langle S^2 \rangle$  according to the Yamaguchi approach [Equation (1)],<sup>[20]</sup> was calculated on the crystal structure coordinates to be  $-724 \text{ cm}^{-1}$ .

$$J = \frac{E_{\text{HS}} - E_{\text{BS}}}{\langle S^2 \rangle_{\text{HS}} - \langle S^2 \rangle_{\text{BS}}} \quad (1)$$

The magnetic susceptibility data recorded on **1** exhibits a slight increase in the magnetic response at temperatures exceeding 200 K (Figure 10). Fitting of this region requires  $J = -545 \text{ cm}^{-1}$  and indicates that the calculated exchange coupling is consistent with the experiment. The more flattened optimized structure leads to a decrease in  $J$  to  $-79 \text{ cm}^{-1}$  and suggests the antiferromagnetic coupling pathways are maximized when the two Cu-centered square planes are orthogonal and when the angles of the  $\text{Cu}_2\text{S}_2$  are acute.

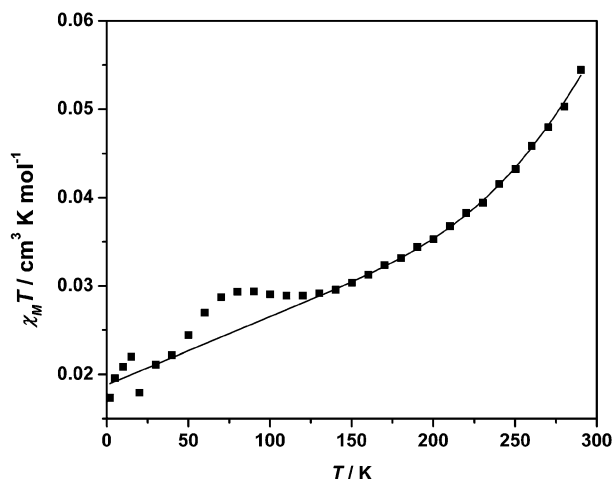
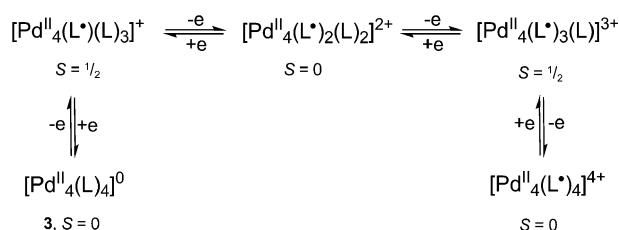


Figure 10. Temperature dependence of the molar magnetic susceptibility times temperature of a solid sample of **1**. The squares represent the experimental data, whereas the solid line represents the best fit to a model described by  $H_{\text{ex}} = -2JS_1S_2$ , where  $S_1 = S_2 = 1/2$ ,  $g = 2.00$ ,  $J = -545 \text{ cm}^{-1}$ . A small contribution from  $\chi_{\text{TIP}} = -77 \times 10^{-6} \text{ cm}^3 \text{ mol}^{-1}$ , seen as a linear slope at  $T < 200 \text{ K}$ , was added to the simulation.

## Conclusions

We synthesized four new polynuclear complexes having varying structural motifs based on the Schiff base N,O,S-donor ligand 2-[(*E*)-2-mercaptophenylimino]methyl-4,6-di-*tert*-butylphenolate(2-). Moreover, we identified a resonance form of  $L^{2-}$  that contributes to the short experimental C–O bond length in complexes **1–4** that is not a consequence of a coordinated phenoxyl. Most remarkably, tetramers **3** and **4** both showed four and six reversible oxidations in their cyclic voltammograms, respectively, that are assigned as ligand centered. These assignments are corroborated by electronic absorption and EPR spectroscopy, even though the spectroscopic changes upon formation of the phenoxyl are subtle because the radical is delocalized across four metal ions and multiple ligands. Thus, we characterize the oxidation products of **3** and **4** as species with *coordinated* phenoxyl ligands. Hence, **3** is the first of a five-membered electron transfer series linked by successive one-electron oxidation of  $L^{2-}$  (Scheme 3). A similar seven-membered electron transfer series can be formulated for **4**.



Scheme 3. Electron transfer series for **3**.

The highest occupied MOs of the copper dimer, **1**, are two SOMOs: the  $\sigma^*$  bond of the  $d_{x^2-y^2}$  orbital. These are antiferromagnetically coupled with a reasonably small integral overlap but the geometry of the complex facilitates a

large singlet–triplet coupling that is calculated at  $J = -724 \text{ cm}^{-1}$ , in agreement with the trend observed at elevated temperatures in the magnetic susceptibility data. Kida et al. reported a similar copper dimer,  $[\text{Cu}^{\text{II}}_2(\text{LONO})_2]^{2-}$ , containing a  $\text{Cu}_2\text{O}_2$  diamond core (Figure 11).<sup>[9]</sup> The magnetic susceptibility data shows an increase in the effective magnetic moment at temperatures  $>100 \text{ K}$ , and the simulation afforded a value for  $J$  ranging from  $-197$  to  $-224 \text{ cm}^{-1}$ .

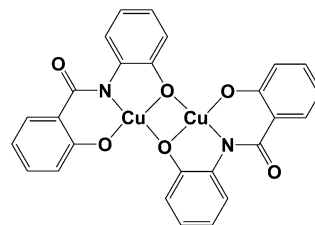


Figure 11. Structure of  $[\text{Cu}^{\text{II}}_2(\text{LONO})_2]^{2-}$  (taken from ref.<sup>[9]</sup>).

The  $\text{Cu}_2\text{O}_2$  diamond core in  $[\text{Cu}^{\text{II}}_2(\text{LONO})_2]^{2-}$  is planar compared with **1**, where the  $\text{Cu}_2\text{S}_2$  unit is puckered such that the copper square planes make an acute angle of  $80.4^\circ$ . It is this near-orthogonality in **1**, compared with the planar  $[\text{Cu}^{\text{II}}_2(\text{LONO})_2]^{2-}$ , from which that large coupling value is obtained.

The chemistry described in this paper further endorses the notion of redox noninnocence amongst Schiff base ligands, and that this particular feature may be central to their role in numerous catalytic applications.

## Experimental Section

**Materials:** All air-sensitive materials were manipulated by using standard Schlenk line techniques or a glove box. The metal salts  $\text{CoCl}_2$ ,  $\text{Cu}(\text{OAc})_2 \cdot \text{H}_2\text{O}$ ,  $\text{Pd}(\text{OAc})_2$ , and  $\text{PtCl}_2$  were purchased from Strem Chemicals and used as received. The ligand 2-[(*E*)-2-mercaptophenylimino]methyl-4,6-di-*tert*-butylphenol ( $\text{H}_2\text{L}$ ) was prepared as detailed in ref.<sup>[8]</sup>

**$[\text{Cu}^{\text{II}}_2(\text{L})_2]$  (**1**):** A pale-yellow solution of  $\text{H}_2\text{L}$  (400 mg, 1.17 mmol) in acetonitrile (40 mL) was treated with  $\text{Cu}(\text{OAc})_2 \cdot \text{H}_2\text{O}$  (234 mg, 1.17 mmol). After 10 min stirring under an atmosphere of argon, triethylamine (0.10 mL, 0.72 mmol) was added by syringe, and the reaction mixture was stirred for 30 min under an atmosphere of argon. The mixture was then exposed to atmosphere and stirred for an additional 2 h, generating a dark green-brown solution. A microcrystalline solid evolved, which was isolated after slow evaporation of the mother liquor. Yield: 0.26 g (55%).  $\text{C}_{42}\text{H}_{50}\text{Cu}_2\text{N}_2\text{O}_2\text{S}_2$  (806.10): calcd. C 62.58, H 6.25, N 3.47, Cu 15.76; found C 62.78, H 6.53, N 3.63, Cu 15.81. MS (ESI):  $m/z = 805 [\text{M} - \text{H}]$ .

**$[\text{Pt}^{\text{II}}_3(\text{L})_3]$  (**2**):** Prepared by following the procedure outlined for **1**.  $\text{H}_2\text{L}$  (200 mg, 0.58 mmol),  $\text{PtCl}_2$  (156 mg, 0.58 mmol), and triethylamine (0.05 mL, 0.36 mmol). Single crystals were grown by slow evaporation of a dichloromethane/acetonitrile (1:1) solution of the complex. Yield: 0.24 g (77%).  $\text{C}_{63}\text{H}_{75}\text{N}_3\text{O}_3\text{Pt}_3\text{S}_3$  (1603.74): calcd. C 47.18, H 4.71, N 2.61, Pt 36.49; found C 47.31, H 4.93, N 2.76, Pt 36.57. MS (ESI):  $m/z = 1602.2 [\text{M} - \text{H}]$ .

**$[\text{Pd}^{\text{II}}_4(\text{L})_4]$  (**3**):** Prepared by following the procedure outlined for **1**.  $\text{H}_2\text{L}$  (500 mg, 1.46 mmol),  $\text{Pd}(\text{OAc})_2$  (330 mg, 1.46 mmol), and triethylamine (0.20 mL, 1.44 mmol). Single crystals were obtained by slow evaporation of an acetonitrile solution of the complex.

Yield: 0.44 g (68%).  $C_{84}H_{100}N_4O_4Pd_4S_4$  (1783.69): calcd. C 56.56, H 5.65, N 3.14, Pd 23.86; found C 56.78, H 5.93, N 3.29, Pd 24.07. MS (ESI):  $m/z$  = 1782.6 [M – H].

[Co<sup>III</sup><sub>4</sub>(L)<sub>6</sub>] (**4**): Prepared by following the procedure outlined for **1**. H<sub>2</sub>L (500 mg, 1.46 mmol), CoCl<sub>2</sub> (190 mg, 1.46 mmol), and triethylamine (0.20 mL, 1.44 mmol) in the presence of air. Single crystals were grown by slow evaporation of a dichloromethane/acetonitrile (1:1) solution of the complex. Yield: 0.42 mg (76% based on L).  $C_{126}H_{150}Co_4N_6O_6S_6$  (2272.74): calcd. C 66.58, H 6.65, N 3.70, Co 10.37; found C 66.09, H 6.57, N 3.47, Co 10.05. MS (ESI):  $m/z$  = 2270.8 [M – H].

**Calculations:** All DFT calculations were performed with the ORCA program package.<sup>[21]</sup> Truncated **1**, with *t*Bu groups removed, was geometry optimized by using the B3LYP functional.<sup>[22]</sup> The all-electron basis sets were those reported by the Ahlrichs group.<sup>[23,24]</sup> Triple- $\zeta$ -quality basis sets with one set of polarization functions (TZVP) was used for all non-carbon and non-hydrogen atoms. The carbon and hydrogen atoms were described by slightly smaller polarized split-valence SV(P) basis sets that are double- $\zeta$ -quality in the valence region and contain a polarizing set of d functions on the non-hydrogen atoms.<sup>[23]</sup> Auxiliary basis sets used to expand the electron density in the calculations were chosen to match the orbital basis. The self-consistent field calculations were tightly converged ( $1 \times 10^{-8}$   $E_h$  in energy,  $1 \times 10^{-7}$   $E_h$  in the density charge, and  $1 \times 10^{-7}$  in the maximum element of the DIIS<sup>[25]</sup> error vector). The geometry search for all complexes was carried out in redundant internal coordinates without imposing geometry constraints. Corresponding<sup>[26]</sup> and quasi-restricted<sup>[27]</sup> orbitals and density plots were obtained by using Molekel.<sup>[28]</sup> We describe our computational result for **1** by using the broken symmetry (BS) approach.<sup>[29]</sup>

**X-ray Crystallographic Data Collection and Refinement:** Single crystals of compounds **1** to **4** were coated with perfluoropolyether, picked up with nylon loops, and immediately mounted in the nitrogen cold stream of a Bruker-Nonius KappaCCD diffractometer equipped with a Mo-target rotating-anode X-ray source. Graphite monochromated Mo- $K_\alpha$  radiation ( $\lambda$  = 0.71073 Å) was used throughout. Final cell constants were obtained from least-squares

fits of all measured reflections. Intensity data of **1**, **2**, and **4** were corrected for absorption by using intensities of redundant reflections by using SADABS.<sup>[30]</sup> The data set of compound **3** was corrected with the Gaussian-type absorption correction method embedded in XPREP.<sup>[31]</sup> The structures were readily solved by Patterson methods and subsequent difference Fourier techniques. The Siemens SHELXTL<sup>[31]</sup> software package was used for solution and artwork of the structures, SHELXL97,<sup>[32]</sup> was used for the refinement. All non-hydrogen atoms were anisotropically refined and hydrogen atoms were placed at calculated positions and refined as riding atoms with isotropic displacement parameters, except for some methyl hydrogen atoms in disordered acetonitrile molecules of crystallization, which could not be reliably located. Crystallographic data of the compounds are listed in Table 4. The position of an acetonitrile solvent molecule in compound **2** was found to be mixed-up with a minor amount of dichloromethane ( $\approx 31\%$ ). A split atom model with constrained bond lengths and angles by using the DFIX instruction of SHELXL97 was used. Equal anisotropic displacement parameters were assigned to disordered neighboring split atoms. Three out of six acetonitrile molecules of crystallization in **3** were also treated similarly as a result of their disorder. A total of 22 restraints were used. Some acetonitrile molecules in **4** were treated the same way, as they were found to be severely disordered, 36 restraints were used here. CCDC-720613 (for **1**), -720614 (for **2**), -720615 (for **3**), and -720616 (for **4**) contain the supplementary crystallographic data for this paper. These data can be obtained free of charge from The Cambridge Crystallographic Data Centre via [www.ccdc.cam.ac.uk/data\\_request/cif](http://www.ccdc.cam.ac.uk/data_request/cif).

**Physical Measurements:** Cyclic and square-wave voltammograms were recorded with an EG&G potentiostat/galvanostat in CH<sub>2</sub>Cl<sub>2</sub> solutions {0.10 M [N(*n*Bu)<sub>4</sub>]PF<sub>6</sub>} at a glassy carbon working electrode. Ferrocene was used as an internal standard; all redox potentials are given versus the ferrocenium/ferrocene (Fc<sup>+</sup>/Fc) couple. Electronic absorption spectra from spectroelectrochemical measurements were obtained by using a Hewlett–Packard HP 8452A diode array spectrophotometer (200–1100 nm). X-band EPR spectra were recorded with a Bruker ESP 300 spectrometer and simulated by using ESIM developed by Dr. E. Bill. Elemental analyses

Table 4. Crystallographic data for **1**·MeCN, **2**·1.7MeCN·0.3CH<sub>2</sub>Cl<sub>2</sub>, **3**·6MeCN, and **4**·10MeCN.

	<b>1</b> ·MeCN	<b>2</b> ·1.7MeCN·0.3CH <sub>2</sub> Cl <sub>2</sub>	<b>3</b> ·6MeCN	<b>4</b> ·10MeCN
Formula	C <sub>44</sub> H <sub>53</sub> Cu <sub>2</sub> N <sub>3</sub> O <sub>2</sub> S <sub>2</sub>	C <sub>66</sub> H <sub>80.7</sub> Cl <sub>0.6</sub> N <sub>4.7</sub> O <sub>3</sub> Pt <sub>3</sub> S <sub>3</sub>	C <sub>96</sub> H <sub>118</sub> N <sub>10</sub> O <sub>4</sub> Pd <sub>4</sub> S <sub>4</sub>	C <sub>146</sub> H <sub>180</sub> Co <sub>4</sub> N <sub>16</sub> O <sub>6</sub> S <sub>6</sub>
<i>F</i> <sub>w</sub>	847.09	1698.98	2029.84	2683.14
Space group	<i>P</i> $\bar{1}$ , No. 2	<i>P</i> $\bar{1}$ , No. 2	<i>P</i> 2 <sub>1</sub> / <i>n</i> , No. 14	<i>P</i> 2 <sub>1</sub> / <i>c</i> , No. 14
<i>a</i> / Å	9.9829(4)	13.0102(7)	11.8074(7)	31.4781(9)
<i>b</i> / Å	14.4719(6)	15.9188(9)	41.047(3)	19.1055(5)
<i>c</i> / Å	14.6213(5)	18.5944(12)	20.9853(14)	24.2981(7)
$\alpha$ / °	82.279(2)	105.568(4)	90	90
$\beta$ / °	83.934(2)	108.148(4)	102.754(5)	94.693(3)
$\gamma$ / °	88.650(2)	103.507(4)	90	90
<i>V</i> / Å <sup>3</sup>	2081.40(14)	3306.8(3)	9919.8(11)	14564.0(7)
<i>Z</i>	2	2	4	4
<i>T</i> / K	100(2)	100(2)	150(2)	100(2)
$\rho$ (calcd.) / g cm <sup>−3</sup>	1.352	1.706	1.359	1.224
Refl. collected, $2\theta_{\max}$ / °	27216, 52.00	29902, 52.00	42858, 46.54	74048, 45.00
Unique refl., $I > 2\sigma(I)$	8141, 5652	12804, 9516	13164, 8798	18973, 12411
No. of params, restr.	491, 0	760, 6	1090, 22	1552, 36
$\lambda$ / Å, $\mu(K_a)$ / cm <sup>−1</sup>	0.71073, 11.61	0.71073, 64.96	0.71073, 8.50	0.71073, 5.91
<i>R</i> <sub>1</sub> , <sup>[a]</sup> goodness of fit <sup>[b]</sup>	0.0627, 1.068	0.0617, 1.045	0.0721, 1.127	0.0678, 1.026
<i>wR</i> <sub>2</sub> , <sup>[c]</sup> [ $I > 2\sigma(I)$ ]	0.0969	0.1394	0.1274	0.1494
Residual density / e Å <sup>−3</sup>	+0.49, −0.48	+3.14, −2.79	+0.75, −0.72	+1.37, −0.61

[a] Observation criterion:  $I > 2\sigma(I)$ .  $R_1 = \sum ||F_o| - |F_c|| / \sum |F_o|$ . [b] GooF =  $[\sum (w(F_o^2 - F_c^2)(n - p))]^{1/2}$ . [c]  $wR_2 = \{\sum [w(F_o^2 - F_c^2)] / \sum [w(F_o^2)]\}^{1/2}$ , where  $w = 1/(\sigma^2(F_o^2) + (aP)^2 + bP)$ ,  $P = (F_o^2 + 2F_c^2)/3$ .



were performed by H. Kolbe at the Microanalytischen Labor in Mülheim an der Ruhr, Germany. Variable temperature magnetization measurements (4–300 K) were performed with a SQUID magnetometer (MPMS Quantum Design) at a 1 T field. The experimental susceptibility data were corrected for underlying diamagnetism using Pascals's constants.

**Supporting Information** (see footnote on the first page of this article): CV of **1**; electronic absorption spectra of **1** and **2**; calculated bond lengths of **1**.

## Acknowledgments

We thank Dr. Eckhard Bill for useful discussions. N.R. and S.S. are grateful to the Max Planck Society for a doctoral stipend and postdoctoral fellowship, respectively. We thank the Fonds der Chemischen Industrie for financial support.

- [1] a) K. C. Gupta, A. K. Sutar, *Coord. Chem. Rev.* **2008**, 252, 1420–1450; b) P. G. Cozzi, *Chem. Soc. Rev.* **2004**, 33, 410–421.
- [2] M. D. Hobday, T. D. Smith, *Coord. Chem. Rev.* **1973**, 9, 311–337.
- [3] a) L. A. Hoferkamp, K. A. Goldsby, *Chem. Mater.* **1989**, 1, 348–352; b) M. Vilas-Boas, C. Freire, B. de Castro, P. A. Christensen, A. R. Hillman, *Inorg. Chem.* **1997**, 36, 4919–4929.
- [4] a) F. Azevedo, M. A. A. F. de C. T. Carrondo, B. de Castro, M. Convery, D. Domingues, C. Freire, M. T. Duarte, K. Nielsen, I. C. Santos, *Inorg. Chim. Acta* **1994**, 219, 43–54; b) M. A. A. F. de C. T. Carrondo, B. de Castro, A. M. Coelho, D. Domingues, C. Freire, J. Morais, *Inorg. Chim. Acta* **1993**, 205, 157–166; c) B. de Castro, C. Freire, *Inorg. Chem.* **1990**, 29, 5113–5119; d) B. de Castro, C. Freire, E. Pereira, *J. Chem. Soc., Dalton Trans.* **1994**, 571–576; e) C. Freire, B. de Castro, *J. Chem. Soc., Dalton Trans.* **1998**, 1491–1498; f) K. A. Goldsby, J. K. Blaho, L. A. Hoferkamp, *Polyhedron* **1989**, 8, 113–115; g) A. Kapturkiewicz, B. Behr, *Inorg. Chim. Acta* **1983**, 69, 247–251.
- [5] Y. Shimazaki, F. Tani, K. Fukui, Y. Naruta, O. Yamauchi, *J. Am. Chem. Soc.* **2003**, 125, 10512–10513.
- [6] Y. Shimazaki, T. Yajima, F. Tani, S. Karasawa, K. Fukui, Y. Naruta, O. Yamauchi, *J. Am. Chem. Soc.* **2007**, 129, 2559–2568.
- [7] a) P. Guerriero, S. Tamburini, P. A. Vigato, *Coord. Chem. Rev.* **1995**, 139, 17–243; b) P. A. Vigato, S. Tamburini, L. Bertolo, *Coord. Chem. Rev.* **2007**, 251, 1311–1492.
- [8] N. Roy, S. Sproules, T. Weyhermüller, K. Wieghardt, *Inorg. Chem.* **2009**, 48, 3783–3791.
- [9] M. Koikawa, H. Okawa, N. Matsumoto, M. Gotoh, S. Kida, T. Kohzuma, *J. Chem. Soc., Dalton Trans.* **1989**, 2089–2094.
- [10] D. Song, S. Wang, *J. Organomet. Chem.* **2002**, 648, 302–305.
- [11] D. Sellmann, D. Haeussinger, F. W. Heinemann, *Eur. J. Inorg. Chem.* **1999**, 1715–1725.
- [12] C. A. Ghilardi, S. Midollini, A. Orlandini, G. Scapacci, A. Vacca, *J. Organomet. Chem.* **1993**, 461, C4–C6.
- [13] a) B. Castro, C. Freire, M. T. Duarte, M. F. M. Piedade, I. C. Santos, *Acta Crystallogr., Sect. C* **2001**, 57, 370–372; b) W. Sawodny, U. Thewalt, E. Potthoff, R. Ohl, *Acta Crystallogr., Sect. C* **1999**, 55, 2060–2061.
- [14] G. Rajsekhar, C. P. Rao, P. K. Saarenketo, E. Kolehmainen, K. Rissanen, *Inorg. Chem. Commun.* **2002**, 5, 649–652.
- [15] a) B. Adam, E. Bill, E. Bothe, B. Goerd, G. Haselhorst, K. Hildenbrand, S. Sokolowski, S. Steenken, T. Weyhermüller, K. Wieghardt, *Chem. Eur. J.* **1997**, 3, 308–319; b) L. Benisvy, E. Bill, A. J. Blake, D. Collison, E. S. Davies, C. D. Garner, C. I. Guindy, E. J. L. McInnes, G. McArdle, J. McMaster, C. Wilson, J. Wolowska, *Dalton Trans.* **2004**, 3647–3653; c) J. Müller, A. Kikuchi, E. Bill, T. Weyhermüller, P. Hildebrandt, L. Ould-Moussa, K. Wieghardt, *Inorg. Chim. Acta* **2000**, 297, 265–277; d) A. K. Nairn, S. J. Archibald, R. Bhalla, B. C. Gilbert, E. J. MacLean, S. J. Teat, P. H. Walton, *Dalton Trans.* **2006**, 172–176; e) A. K. Nairn, R. Bhalla, S. P. Foxon, X. Liu, L. J. Yellowlees, B. C. Gilbert, P. H. Walton, *J. Chem. Soc., Dalton Trans.* **2002**, 1253–1255.
- [16] a) J. A. Halfen, B. A. Jazdzewski, S. Mahapatra, L. M. Berreau, E. C. Wilkinson, L. Que Jr, W. B. Tolman, *J. Am. Chem. Soc.* **1997**, 119, 8217–8227; b) A. Sokolowski, B. Adam, T. Weyhermüller, A. Kikuchi, K. Hildenbrand, R. Schnepf, P. Hildebrandt, E. Bill, K. Wieghardt, *Inorg. Chem.* **1997**, 36, 3702–3710.
- [17] L. Benisvy, R. Bittl, E. Bothe, C. D. Garner, J. McMaster, S. Ross, C. Teutloff, F. Neese, *Angew. Chem. Int. Ed.* **2005**, 44, 5314–5317.
- [18] a) P. Ghosh, A. Begum, D. Herebian, E. Bothe, K. Hildenbrand, T. Weyhermüller, K. Wieghardt, *Angew. Chem. Int. Ed.* **2003**, 42, 563–567; b) D. Herebian, E. Bothe, F. Neese, T. Weyhermüller, K. Wieghardt, *J. Am. Chem. Soc.* **2003**, 125, 9116–9128; c) S. Kokatam, T. Weyhermüller, E. Bothe, P. Chaudhuri, K. Wieghardt, *Inorg. Chem.* **2005**, 44, 3709–3717; d) K. S. Min, T. Weyhermüller, E. Bothe, K. Wieghardt, *Inorg. Chem.* **2004**, 43, 2922–2931; e) K. Ray, T. Weyhermüller, F. Neese, K. Wieghardt, *Inorg. Chem.* **2005**, 44, 5345–5360.
- [19] F. E. Mabbs, D. Collison, *Electron Paramagnetic Resonance of d Transition Metal Compounds*, Elsevier, Amsterdam, **1992**.
- [20] a) T. Soda, Y. Kitagawa, T. Onishi, Y. Takano, Y. Shiget, H. Nagao, Y. Yoshioka, K. Yamaguchi, *Chem. Phys. Lett.* **2000**, 319, 223–230; b) K. Yamaguchi, Y. Takahara, T. Fueno in *Applied Quantum Chemistry* (Ed.: V. H. Smith), Reidel, Dordrecht, The Netherlands, **1986**, p. 155.
- [21] F. Neese, Neese, F. Orca, *An Ab initio, Density Functional and Semiempirical Electronic Structure Program Package*, version 2.6, revision 35, University of Bonn, Bonn, Germany, **2008**.
- [22] a) A. D. Becke, *J. Chem. Phys.* **1993**, 98, 5648–5652; b) C. T. Lee, W. T. Yang, R. G. Parr, *Phys. Rev. B* **1988**, 37, 785–789.
- [23] A. Schäfer, H. Horn, R. Ahlrichs, *J. Chem. Phys.* **1992**, 97, 2571–2578.
- [24] A. Schäfer, C. Huber, R. Ahlrichs, *J. Chem. Phys.* **1994**, 100, 5829–5835.
- [25] a) P. Pulay, *Phys. Chem. Lett.* **1980**, 73, 393–398; b) P. Pulay, *J. Comput. Chem.* **1982**, 3, 556–560.
- [26] F. Neese, *J. Phys. Chem. Solids* **2004**, 65, 781–785.
- [27] J. C. Schöneboon, F. Neese, W. Thiel, *J. Am. Chem. Soc.* **2005**, 127, 5840–5853.
- [28] Molekel, *Advanced Interactive 3D-Graphics for Molecular Sciences*, Swiss National Supercomputing Center: <http://www.cscs.ch/molekel>.
- [29] a) L. Noodleman, *J. Chem. Phys.* **1981**, 74, 5737–5743; b) L. Noodleman, D. A. Case, A. Aizman, *J. Am. Chem. Soc.* **1988**, 110, 1001–1005; c) L. Noodleman, E. R. Davidson, *Chem. Phys.* **1986**, 109, 131–143; d) L. Noodleman, J. G. Norman, J. H. Osborne, A. Aizman, D. A. Case, *J. Am. Chem. Soc.* **1985**, 107, 3418–3426; e) L. Noodleman, C. Y. Peng, D. A. Case, J. M. Monesca, *Coord. Chem. Rev.* **1995**, 144, 199–244; f) N. Roy, S. Sproules, E. Bill, T. Weyhermüller, K. Wieghardt, *Inorg. Chem.* **2008**, 47, 10911–10920.
- [30] G. M. Sheldrick, *SADABS*, version 2006/1, University of Göttingen, Göttingen, Germany, **2006**.
- [31] *SHELXTL 6.14*, Bruker AXS Inc., Madison, Wisconsin, USA, **2003**.
- [32] G. M. Sheldrick, *SHELXL97*, University of Göttingen, Göttingen, Germany, **1997**.

Received: February 18, 2009  
Published Online: May 11, 2009